

Electronic Supplementary Information

ZIF-derived frame-in-Cage hybrids of ZnSe-CdSe embedded within N-doped carbon matrix for efficient photothermal conversion of CO₂ into fuel

Wei Han, Yajie Chen*, Yuzhen Jiao, Shumei Liang, Wei Li, Guohui Tian*

Key Laboratory of Functional Inorganic Material Chemistry, Ministry of Education of the People's Republic of China, Heilongjiang University, Harbin 150080 P. R. China.

E-mail: tiangh@hlju.edu.cn; chenyajie1970@163.com

Experimental section

1. Preparation of ZnO nanoparticles

The obtained ZIF-8 precursors were placed in muffle furnace and heated to 420 °C with a ramping rate of 2 °C min⁻¹ and then maintained at 420 °C for 2 h in air atmosphere. Finally, the solid ZnO nanocages were obtained.

2. Preparation of ZnSe nanoparticles

In the typical procedure, the 25 mg of selenium powder and 15 mg of NaBH₄ were dispersed in 20 mL of ethanol. The as-prepared ZnO powder was slowly added to the above mixed solution and stirred vigorously for 30 minutes. Finally, the obtained mixture was transferred into Teflon-lined stainless-steel autoclave (40 mL of capacity) at 180 °C for 6 h. After cooling to room temperature, the production was collected by centrifugation, washed several times with deionized water and ethanol, respectively, and dried in an oven for 8 h at 60 °C.

3. Synthesis of ZnSe-CdSe nanoparticles

The conversion of ZnSe nanoparticles to ZnSe-CdSe nanoparticles and CdSe nanoparticles was realized through a cation exchange reaction with the assistance of

ascorbic acid. Typically, The $\text{CdCl}_2 \cdot 2.5 \text{ H}_2\text{O}$ and 20 mg of ascorbic acid were dissolved in 30 mL methanol solution, and ZnSe nanoparticles were then dispersed in the above solution. After stirring for 5 minutes, the resulting mixture was transferred into a 40 mL Teflon-lined autoclave and heated at 160 °C for different time (6 and 10 h) to prepared ZnSe-CdSe nanoparticles and CdSe nanoparticles.

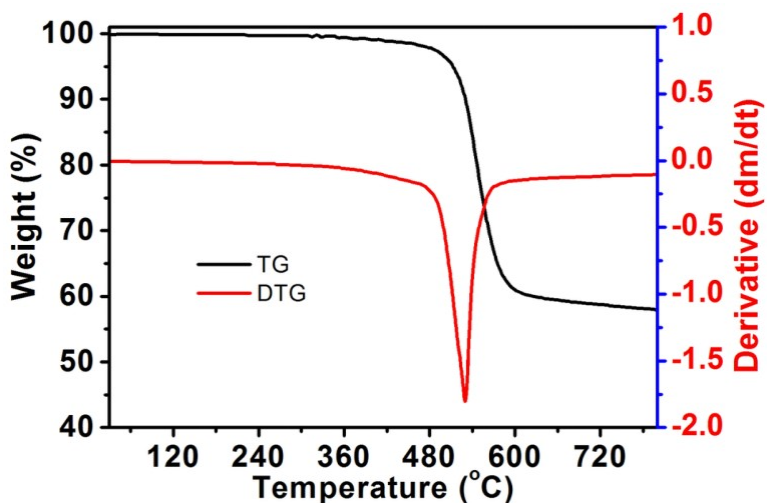


Fig. S1 TG and corresponding DTG curves of ZIF-8 under N_2 gas flow of 20 mL min⁻¹ at a ramp rate of 2 °C min⁻¹.

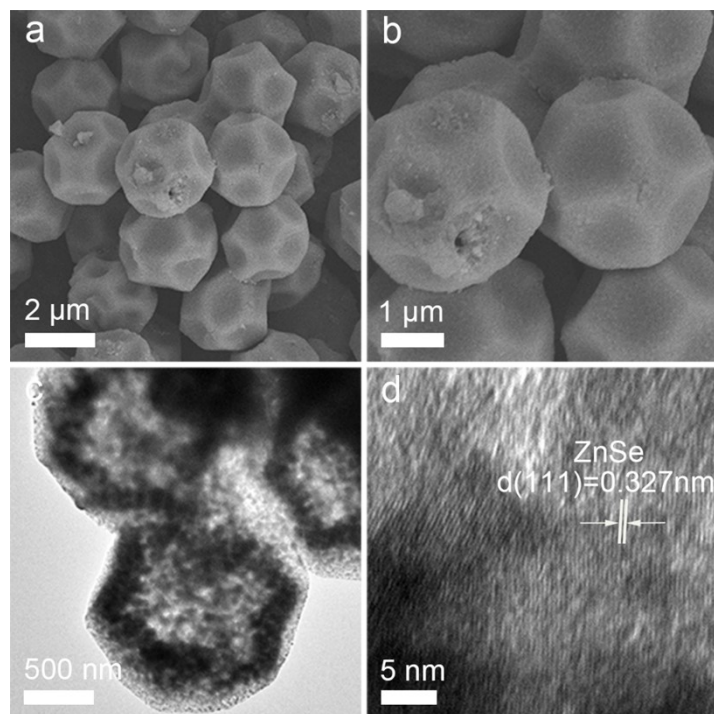


Fig. S2 (a,b) SEM, (c) TEM, and (d) HRTEM images of ZnSe@NC cages.

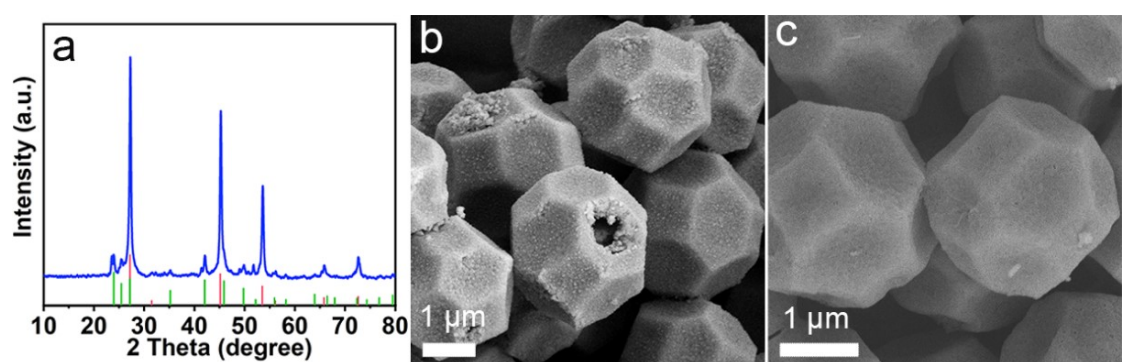


Fig. S3 (a) XRD pattern, (b,c) SEM images of ZnSe-CdSe@NC FC particles in the absence of ascorbic acid.

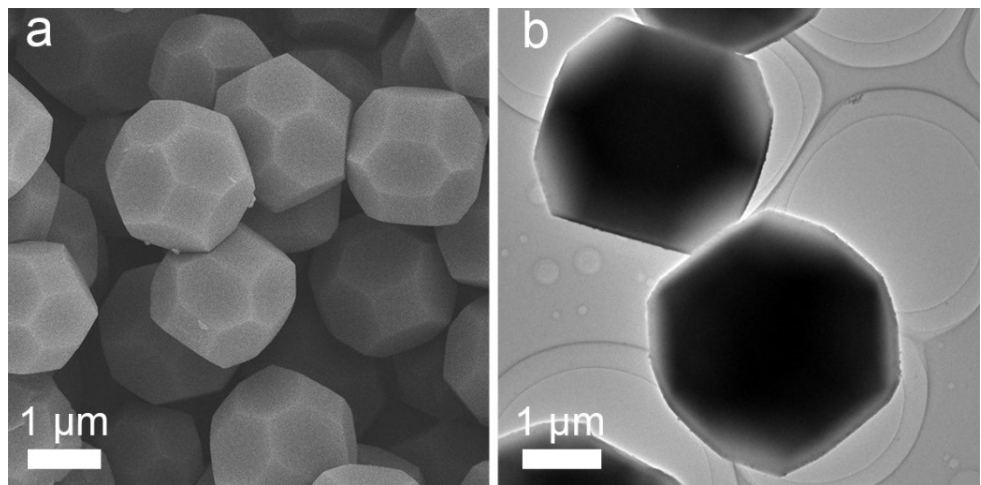


Fig. S4 (a) SEM image, (b) TEM image of ZIF-8.

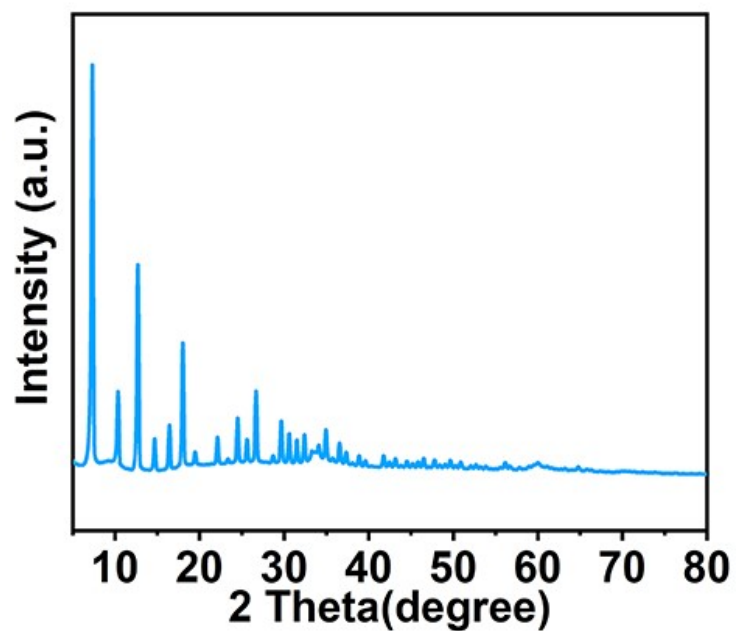


Fig. S5 XRD pattern of ZIF-8.

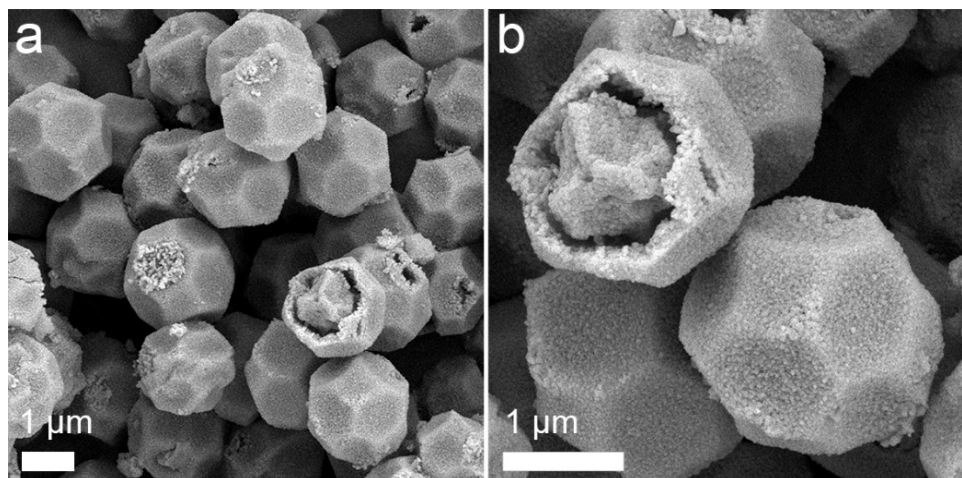


Fig. S6 (a,b) SEM images of ZnSe@NC FC particles.

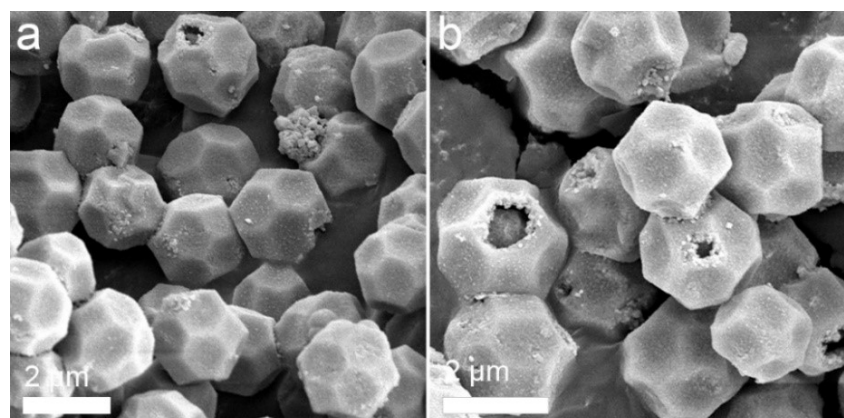


Fig. S7 SEM images of CdSe@NC FC particles.

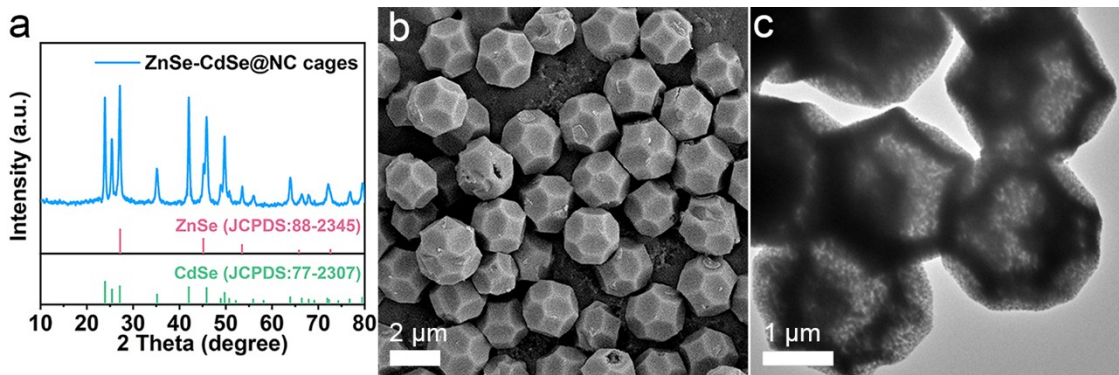


Fig. S8 (a) XRD pattern, (b) SEM image and (c) TEM image of ZnSe-CdSe@NC cages.

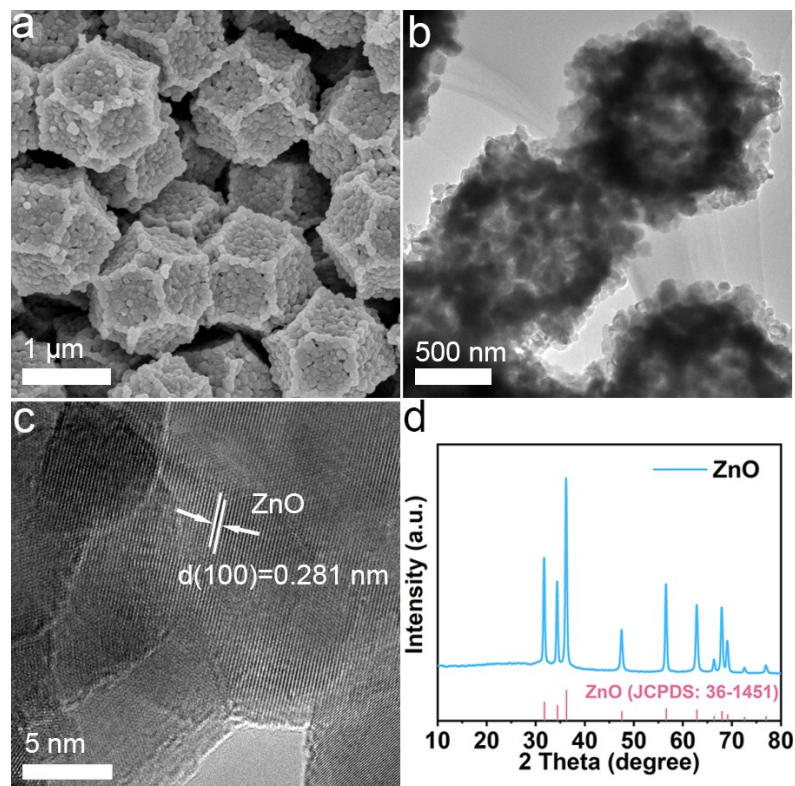


Fig. S9 SEM (a), TEM (b) and HRTEM (c) images, and XRD pattern (d) of ZnO cages.

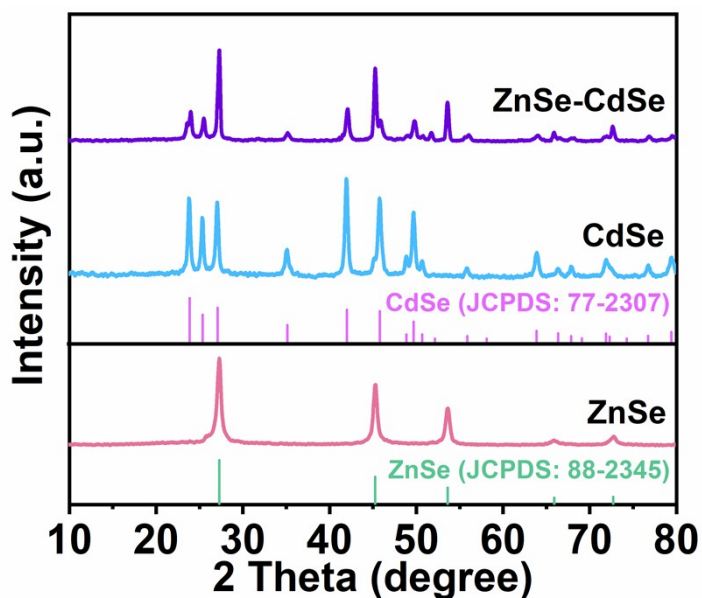


Fig. S10 XRD patterns of ZnSe, CdSe, and ZnSe-CdSe.

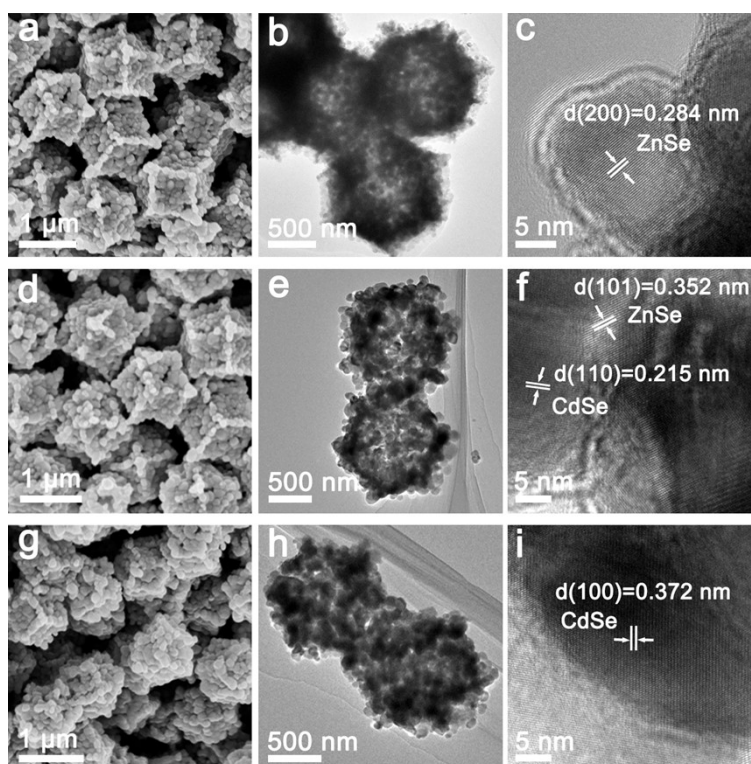


Fig. S11 (a), (b), and (c) are the SEM, TEM, and HRTEM images of ZnSe, respectively; (d), (e), and (f) are the SEM, TEM, and HRTEM images of ZnSe-CdSe, respectively; (g), (h), and (i) are the SEM, TEM, and HRTEM images of CdSe, respectively.

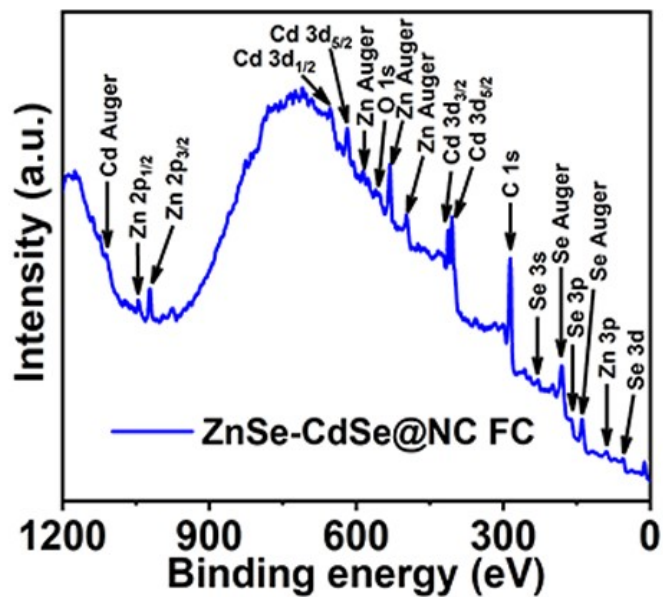


Fig. S12 Wide-scan XPS spectrum of ZnSe-CdSe@NC FC particles.

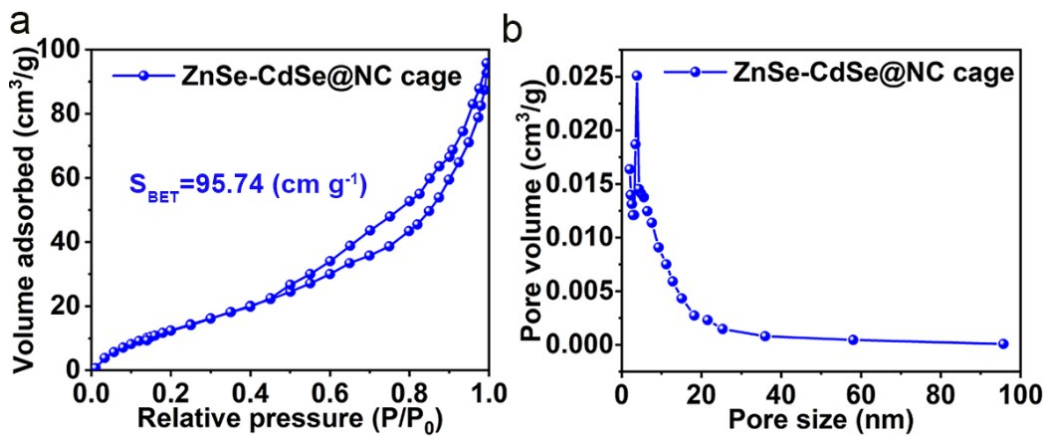


Fig. S13 (a) Nitrogen adsorption-desorption isotherms, (b) Pore size distribution of ZnSe-CdSe@NC cages.

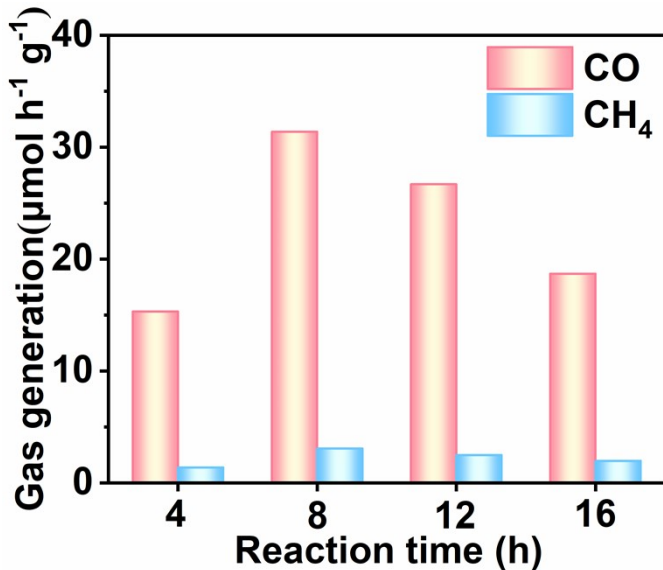


Fig. S14 Performance plot of the ZnSe @NC FC particles after different cation-exchange time (4, 8, 12, and 16 h). The products obtained from cation-exchange time of 4, 8, 12, and 16 h were denoted as ZnSe-CdSe@NC FC-1/2, ZnSe-CdSe@NC FC, ZnSe-CdSe@NC FC-2, and CdSe@NC FC, respectively.

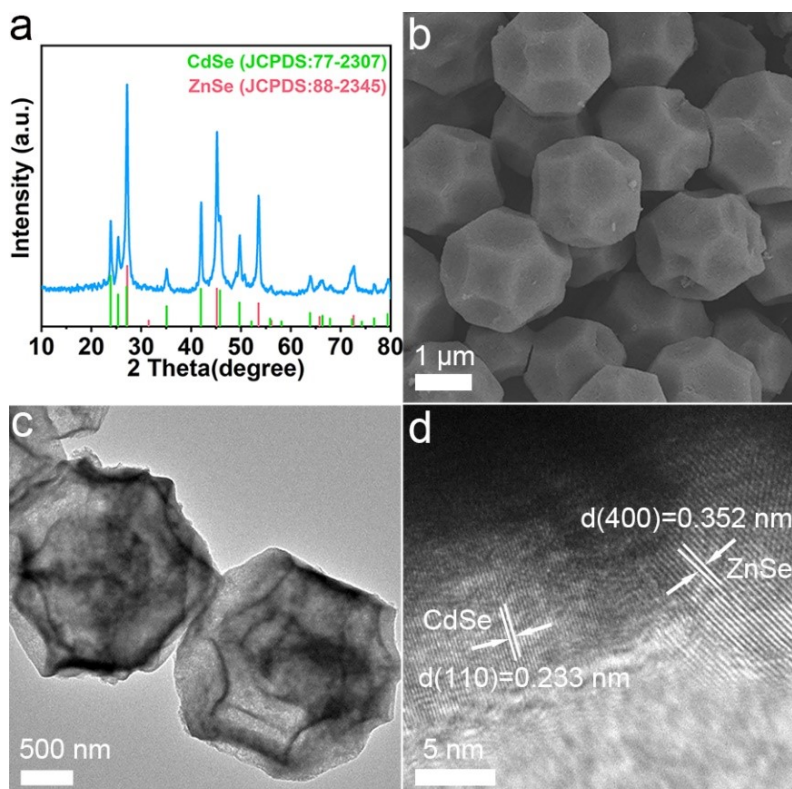


Fig. S15 (a) XRD pattern, (b) SEM, (c) TEM, and (d) HRTEM images of ZnSe-CdSe@NC FC particles after CO_2 reduction reaction tests.

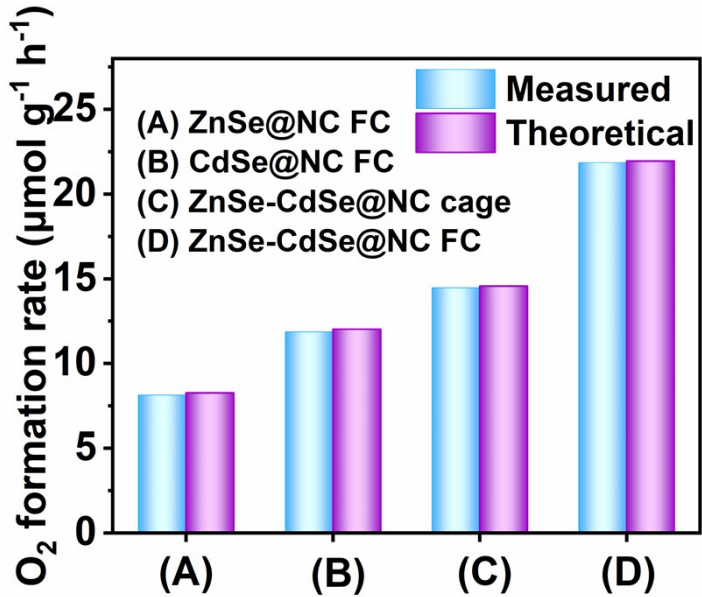


Fig. S16 The O_2 formation rate of different photocatalysis. The air residuals (N_2+O_2) was tested before light irradiation in each experiment. The O_2 generation was obtained by subtracting the air residuals. The theoretical of O_2 formation was calculated by $(\text{O}_2 \text{ formation rate}) = [(\text{CO formation rate})/2 + (\text{CH}_4 \text{ formation rate}) \times 2]$.

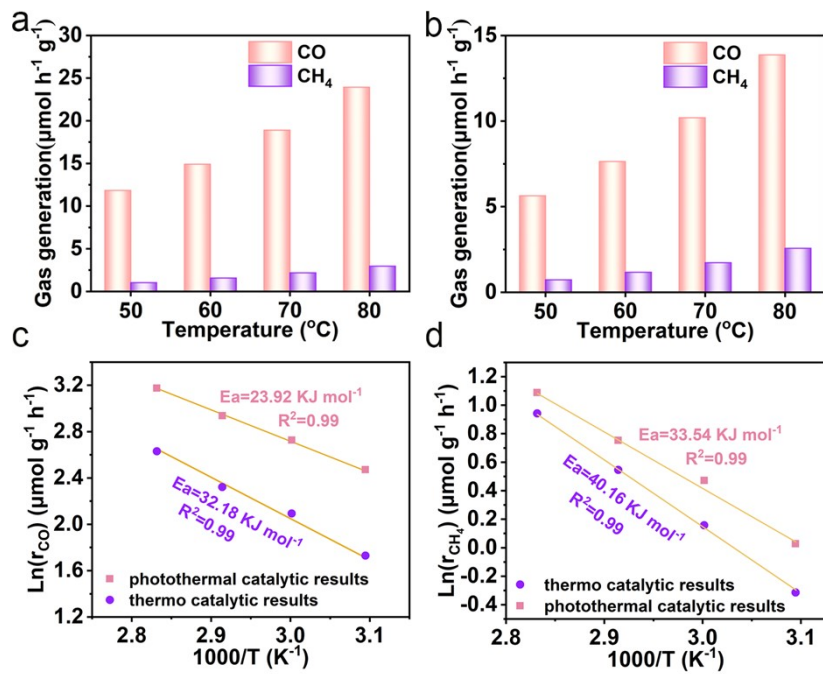


Fig. S17 Thermal catalytic performance of ZnSe-CdSe@NC FC under (a) photothermal catalysis and (b) thermal catalysis. Arrhenius plots of photothermal and thermal catalysis (c) CO and (d) CH₄ generation over ZnSe-CdSe@NC FC catalyst.

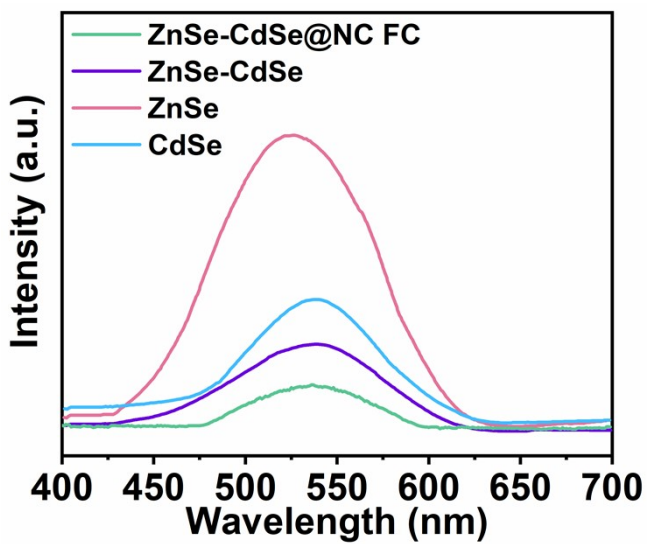


Fig. S18 Steady-state fluorescence spectra of different samples.

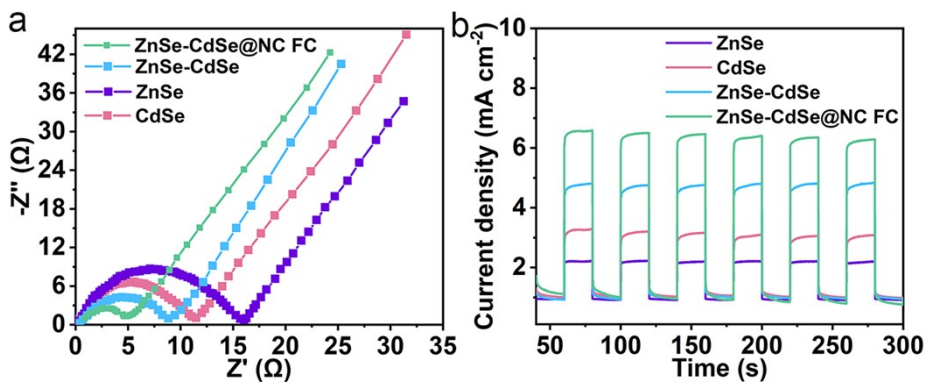


Fig. S19 (a) Nyquist plots and (b) transient photocurrent plots of different samples.

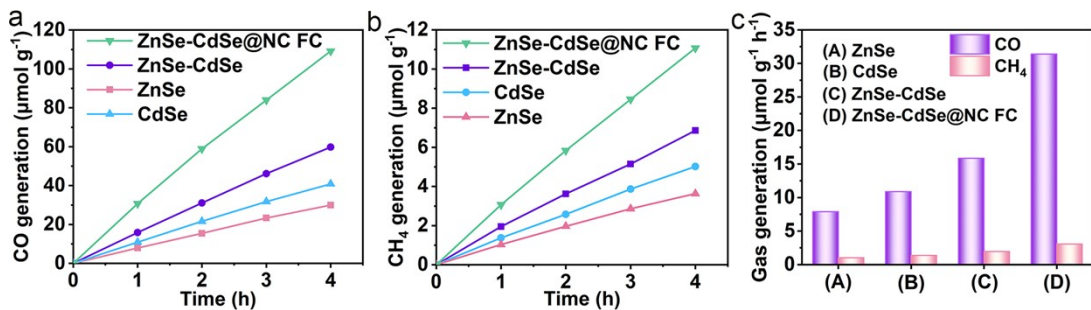


Fig. S20 (a,b) CO and CH₄ yields over different samples, (c) average evolution yields of CO and CH₄ over different samples.

Table S1 Summary of the specific surface area (S_{BET}), pore volume and average pore size of the prepared samples

Samples	Surface area ($\text{m}^2 \text{ g}^{-1}$)	Pore volume ($\text{cm}^3 \text{ g}^{-1}$)	Average pore size (nm)
ZnSe@NC FC	116.64	0.119	10.62
CdSe@NC FC	127.93	0.115	8.89
ZnSe-CdSe@NC FC	157.78	0.216	13.38

Table S2 Gas generation rate and CO selectivity of as-prepared samples

Photocatalyst	CO Yield (μmol $\text{g}^{-1} \text{ h}^{-1}$)	CH_4 Yield (μmol $\text{g}^{-1} \text{ h}^{-1}$)	CO selectivity (%)	CE(%), $\lambda=420$ nm	QE(%), $\lambda=420$ nm	QE(%), $\lambda=550$ nm	QE(%), $\lambda=980$ nm
ZnSe@NC FC	11.08	1.36	68.22	0.007	0.387	0.296	0.166
CdSe@NC FC	16.60	1.86	69.05	0.011	0.563	0.430	0.241
ZnSe-CdSe@NC FC	31.62	3.07	72.09	0.019	1.029	0.786	0.441
ZnSe-CdSe@NC cages	20.53	2.15	70.47	0.013	0.683	0.521	0.292

Calculation of Apparent Quantum Yield (QE %):

The apparent quantum yield (QE) is defined as the ratio of number of reacted electrons to the number of incident photons. In general, two electrons are required to produce one CO molecule, whereas, eight electrons are needed to produce one CH_4 molecule. The apparent quantum yield (QE) measurement was performed using the equation below:

$$QE (\%) = \frac{2 \times N_a \times N_{(\text{CO})} + 8 \times N_a \times N_{(\text{CH}_4)}}{I \times A \times \frac{\lambda}{hc} \times t} \times 100\%$$

where, $N_{(\text{CO})}$ is number of CO (mole) evolved and $N_{(\text{CH}_4)}$ is number of CH_4 (mole) evolved in time “ t ” (1 h), N_a is Avogadro’s number ($N = 6.022 \times 10^{23} \text{ mol}^{-1}$), I is the

incident solar irradiance ($I = 1.5 \text{ mW cm}^{-2}$), 420 nm LED (5 W, Beijing Perfectlight Technology Co. Ltd., China) was positioned 4.0 cm above the reactor, and the focused areas in the reactor for LED was 2.5 cm^2 . λ is the wavelength of the present study (420 nm, 550 nm and 980 nm), h is Planck's constant ($6.62 \times 10^{-34} \text{ J}\cdot\text{s}$), c is the speed of light ($3.0 \times 10^8 \text{ m s}^{-1}$).

Energy Conversion Efficiency (CE %):

$$CE (\%) = \frac{\Delta H_{(CO)} \times N_{(CO)} + \Delta H_{(CH_4)} \times N_{(CH_4)}}{I \times A \times t} \times 100\%$$

where, $N_{(CO)}$ is number of CO (mole) evolved and $N_{(CH_4)}$ is number of CH₄ (mole) evolved in time “ t ” (1 h), $\Delta H_{(CO)}$ is heat of combustion of CO ($\Delta H_{(CO)} = 283.0 \text{ kJ mol}^{-1}$) and $\Delta H_{(CH_4)}$ is heat of combustion of CH₄ ($\Delta H_{(CH_4)} = 890.0 \text{ kJ mol}^{-1}$), I is the incident solar irradiance ($I = 100 \text{ mW cm}^{-2}$) over the exposed irradiated area A (2.5 cm^2).

Table S3 Summary of the photoluminescence decay time (τ) and their relative intensities of the different samples

Sample	$\tau_1(\text{ns})$	$\tau_2(\text{ns})$	$I_1(\%)$	$I_2(\%)$	Average lifetime (τ, ns)
ZnSe@NC FC	1.34	7.32	39.86	60.14	6.67
CdSe@NC FC	1.52	8.32	38.62	61.38	7.62
ZnSe-CdSe@NC FC	3.82	13.45	42.68	57.32	11.77

The average lifetime was calculated using equation: $(\tau) = (I_1\tau_1^2 + I_2\tau_2^2)/(I_1\tau_1 + I_2\tau_2)$

Table S4 The determined energy band parameters of samples

Photocatalyst	E_g	E_f	XPS_{VB}	E_{VB}	E_{CB}
ZnSe	2.24	-0.96	1.85	0.89	-1.35
CdSe	1.72	-1.16	2.10	0.93	-0.79

Table S5 Comparison of the activity of ZnSe-CdSe@NC FC in the photocatalytic CO₂ reduction with the catalysts recently reported

Photocatalyst	Reaction medium	Radiation source	Major Products	Yield $\mu\text{mol g}^{-1} \text{h}^{-1}$	Ref.
PNT	H ₂ O vapor	500 W mercury lamp	CO	11.05	[1]
Cu:CsPbBr ₃	H ₂ O vapor	300 W Xe lamp	CH ₄	14.72	[2]
Ni/TiO ₂	H ₂ O vapor	375 W IR lamp	CH ₄	0.4639	[3]
Co@CoN&C	H ₂ O vapor	300 W Xe lamp	CO	0.132	[4]
WO _{3-x}	H ₂ O vapor	300 W Xe lamp	C ₂ H ₄	5.30	[5]
Ni/N-CeO ₂	H ₂ O vapor	300 W Xe lamp	CO	0.0209	[6]
Cs ₃ Sb ₂ I ₉	H ₂ O vapor	200 mW cm ⁻² Xe lamp	CO CH ₄	95.7 2.9	[7]
In ₂ O _{3-x} (OH) _y	H ₂ O vapor	2.2 kW m ⁻² Xe lamp	CO	15	[8]
G-NiO/Ni	H ₂ O vapor	223.6 mW cm ⁻² Xe lamp	CH ₄	642	[9]
m-CN@CsPbBr ₃	CO ₂ and H ₂ O vapor	Xe lamp	CO	42.8	[10]
Pt/Co-Al ₂ O ₃	H ₂ O vapor	500 W Xe lamp	CO H ₂	5.365 4.536	[11]
Rh/Al	H ₂ O vapor	11.3 W cm ⁻² Xe lamp	CH ₄	0.55	[12]
Ag/AgBr/CsPbBr ₃	H ₂ O vapor	300 W Xe lamp	CO	456.15	[13]
Cs ₃ Bi ₂ I ₉	H ₂ O vapor	UV lamp 32W, 305 nm	CO CH ₄	7.8 1.5	[14]
Ni/Nb ₂ C	ethanol	300 W Xe lamp	CO, CH ₄	8.5	[15]

ZnSe-CdSe@NC FC	H ₂ O vapor	300 W Xe lamp	CO	31.62	This work
--------------------	---------------------------	------------------	----	-------	--------------

References

1. C.Y. Xu, W.H. Huang, Z. Li, B.W. Deng, Y.W. Zhang, M.J. Ni, K.F. Cen. *ACS Catal.*, 2018, **8**, 6582-6593.
2. H. Bian, T.F. Liu, D. Li, Z. Xu, J.H. Lian, M. Chen, J.Q. Yan, S.Z. Liu. *Chem. Eng. J.*, 2022, **435**, 135071.
3. Q. Li, Y.X. Gao, M. Zhang, H. Gao, J. Chen, H.P. Jia. *Appl. Catal. B: Environ.*, 2022, **303**, 120905.
4. S.B. Ning, H. Xu, Y.H. Qi, L.Z. Song, Q.Q. Zhang, S.X. Ouyang, J.H. Ye. *ACS Catal.*, 2020, **10**, 4726-4736.
5. Y. Deng, J. Li, R.M. Zhang, C.Q. Han, Y. Chen, Y. Zhou, W. Liu, P.K. Wong, L.Q. Ye. *Chinese J. Catal.*, 2022, **43**, 1230-1237.
6. Z.W. Jia, S.B. Ning, Y.X. Tong, X. Chen, H.L. Hu, L.Q. Liu, J.H. Ye, D.F. Wang. *ACS Appl. Nano Mater.*, 2021, **4**, 10485-10494.
7. Y.Y. Wang, Q.X. Zhou, Y.F. Zhu, D.S. Xu. *Appl. Catal. B: Environ.*, 2021, **294**, 120236.
8. L.B. Hoch, T.E. Wood, P.G. O'Brien, K. Liao, L.M. Reyes, C.A. Mims, G.A. Ozin. *Adv. Sci.*, 2014, **1**, 1400013.
9. H. Szalad, L. Peng, A. Primo, J. Albero, H. Garcia. *ChemComm*, 2021, **57**, 10075-10078.
10. H. Bian, D. Li, S.Y. Wang, J.Q. Yan, S.Z. Liu. *Chem. Sci.*, 2022, **13**, 1335-1341.
11. Z.H. Xie, Y.Z. Li, Z.Y. Zhou, Q.Q. Hu, J.C. Wu, S.W. Wu. *J. Mater. Chem. A*, 2022, **10**, 7099-7110.
12. G. Fu, M.H. Jiang, J. Liu, K.Q. Zhang, Y. Hu, Y. Xiong, A.Y. Tao, Z.X. Tie, Z. Jin. *Nano Lett.*, 2021, **21**, 8824-8830.
13. P. Gao, P. Wang, X.L. Liu, Z.H. Cui, Y.Q. Wu, X.H. Zhang, Q.Q. Zhang, Z.Y. Wang, Z.K. Zheng, H.F. Cheng, Y.Y. Liu, Y. Dai, B.B. Huang. *Catal. Sci. Technol.*, 2022, **12**, 1628-1636.
14. S.S. Bhosale, A.K. Kharade, E. Jokar, A. Fathi, S.M. Chang, E.W-G. Diau. *J. Am. Chem. Soc.*, 2019, **141**, 20434-20442.
15. Z.Y. Wu, C.R. Li, Z. Li, K. Feng, M.J. Cai, D.K. Zhang, S.H. Wang, M.Y. Chu, C.C. Zhang, J.H. Shen, Z. Huang, Y.L. Xiao, G.A. Ozin, X.H. Zhang, L. He. *ACS Nano*, 2021, **15**, 5696-5705.